

Fig. 3 Vane structure with noise reduction modifications.

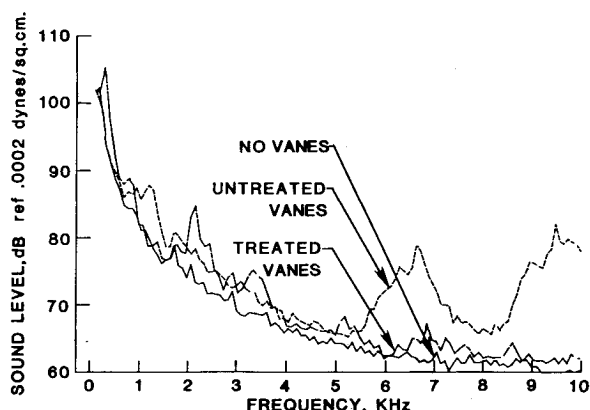


Fig. 4 Background noise spectra for an in-flow microphone with no vanes, untreated vanes, and treated vanes installed [dynamic pressure 2278 Pa (47.6 psf)].

### Noise Reduction Approach

The high-frequency flow noise produced by the vane structure is due to the generation and shedding of vorticity from the hard vane structure. Such self-noise mechanisms are explained in detail in Refs. 6 and 7. The noise reduction modifications to the vane structure are shown in Fig. 3. A thin layer of open-cell polyurethane foam was glued to the downwind surface of each vane. The foam was shaped to have a smooth junction with the structure near the leading edge and to be approximately 2.5 cm (1.0 in.) thick at the trailing edge. This foam served to inhibit vortex generation, as well as to change the vane surface impedance, thus reducing the noise radiation without altering the vanes' desired pulsation suppression characteristics. To make the structure more aerodynamically streamlined, sections of wood dowel were attached to the blunt leading edge of the support rails to create a rounded leading edge. Slender triangular lengths of wood were also attached to the rail trailing edge. All bolt holes, protruding hardware, and sharp corners or steps were filled or covered with clay to avoid cavity noise or "whistles." A boundary-layer trip was applied near the leading edge of the steel rail to prevent the occurrence of the coherent vortex shedding noise attributed to laminar boundary layers.<sup>7</sup>

### Results

The results of these noise reduction modifications are shown in Fig. 4. A comparison of the measured background noise spectra for a microphone located within the flow of the tunnel test section is presented. The spectrum created by the untreated vane structure exhibits two large amplitude humps near 6 and 10 kHz. The result of the vane treatment is to reduce this high-frequency background noise (by as much as 20 dB) to levels comparable to those measured with no vanes

installed. Similar noise reduction results were measured at several other in-flow microphone locations and over a range of tunnel speeds, although the largest noise reduction occurred at the higher tunnel speeds [dynamic pressure of 1200-2400 Pa (25-50 psf)]. On-line observations of the velocity fluctuations confirmed that the pulsation problem was still favorably reduced. Thus, the modifications to the vane structure were verified as an effective, economical, and easily implemented technique to reduce the additional noise induced by the vanes.

### References

- <sup>1</sup>Jacobs, E. N., "Investigation of Air Flow in Open-Throat Tunnels," NACA Rept. 322, 1929.
- <sup>2</sup>Seiferth, R., "Pre-Calculation and Removal of Oscillations in Free-jet Wind Tunnels," *AVA Monographs on German Aeronautical Research Carried Out Since 1939*, Vol. D4.4, Ministry of Aircraft Production, Volkenrode, Rept. and Trans. 947, Aug. 1947.
- <sup>3</sup>Rogers, O.R., "Wind Tunnel Pulsations," AAF Tech. Rept. 5513, 1946.
- <sup>4</sup>Brodski, Z., "Stream Control for Low Speed Range in Wind Tunnels," FTD-TT-62-1476/1+2, March 1985 (unedited rough draft translation).
- <sup>5</sup>Sellers, W.L. III, Applin, Z.T., Molloy J.K., and Gentry G.L., "The Effect of Jet Exit Vanes on Flow Pulsations in an Open Jet Wind Tunnel," NASA TM-86299, 1984.
- <sup>6</sup>Brooks, T.F. and Schlinker, R.H., "Progress in Rotor Broadband Noise Research," *Vertica*, Vol. 7, 1983, pp. 287-307.
- <sup>7</sup>Brooks, T.F. and Marcolini, M.A. "Airfoil Self Noise—Effect of Scale," AIAA Paper 83-0785, 1983.

## Speed Measurement of Flat Flame in a Tube Using Ion Probes

Masao Maekawa\*

Ehime University, Matsuyama, Japan

### Introduction

THE difficulties of measuring flame speed using various types of tubes have been described elsewhere.<sup>1</sup> The difficulties are due to problems in generating a flat flame. In trying to solve this problem, Coward and Hartwell<sup>2</sup> introduced a tube technique that Garstein et al.<sup>3</sup> improved by adding a nozzle to smooth the flow. However, the flame surfaces were semiellipsoids of revolution. Fuller et al.<sup>4</sup> measured the fundamental flame speed of propane-air mixtures by means of multiple-exposure photographs using a modified Garstein tube. Our model is also a modified Garstein tube, but it has ion probes mounted on the tube to measure the flame speeds. The present study was, in fact, undertaken to develop a means of measuring flame speeds directly using ion probes. In this experiment, measurements of the flame speeds made by the ion probes were compared with those made by multiple-exposure photographs of the flame moving down the tube. Using the ion probe method, accurate measurements were easily taken and the results were in agreement with other studies. Therefore, it is thought that the ion probe method of measuring flame speeds can be a useful experimental tool.

Received May 7, 1984; revision received Oct. 25, 1984. Copyright © American Institute of Aeronautics and Astronautics, Inc., 1985. All rights reserved.

\*Department of Mechanical Engineering.

### Experiment

The experimental apparatus used in this study is shown in Fig. 1. The flame tube consists of a nozzle, a quenching screen, ion probes, and electrodes. The screens used for quenching were of 40, 50, and 60 mesh. The flame tube was made from an acrylic resin, 100 mm i.d. and 1000 mm long. The tube was mounted vertically. The top end of the tube was equipped with one of several interchangeable nozzles. The nozzle diameter could be varied in 2 mm increments between 18-30 mm. The nozzle was 50 mm long. Ignition electrodes were inserted as shown in Fig. 1 and were mounted 250 mm below the nozzle. The screen served to quench the flame as it moved up the tube immediately after it had been ignited. The screens were held in place between thin piston rings so that they could be easily interchanged. The power supply for ignition was a high-voltage spark between brass electrodes having a gap spacing of 0.3 mm. High spark energies were available from the power supply, with the energy delivered across the gap instantaneously. The ion probe was set to signal the arrival of the flame. When the flame arrived at the ion probe, the pulse was recorded on the visigraph. Ten ion probes were used, set at 50 mm intervals. The desired propane-air mixture was supplied to the tube at a room temperature of 7°C and at atmospheric pressure. The propane-air mixture of the desired concentration was supplied from the mixing and metering system to the tube. The flame was initiated by discharging the electrodes with the flame generating toward the bottom end and the screen. The ion pulse appeared when the flame arrived at the ion probes.

Table 1 Parameters of flame generation

Equivalence ratio	Mesh	Screen location, <sup>a</sup> mm	Nozzle diameter, mm
0.70	60	50	20
0.75	60	10	18
0.80	50	10	22
0.85	50	50	30
0.90	40	50	26
0.95	40	10	28
1.00	40	50	24

<sup>a</sup>Distance from the ignition electrodes.

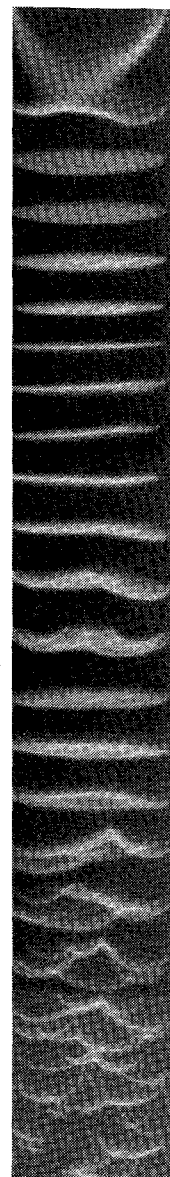


Fig. 2 Multiple-exposure photograph at equivalent ratio of 0.7 (ignition is at top).

Fig. 1 Clamped elastically supported column under partial follower force.

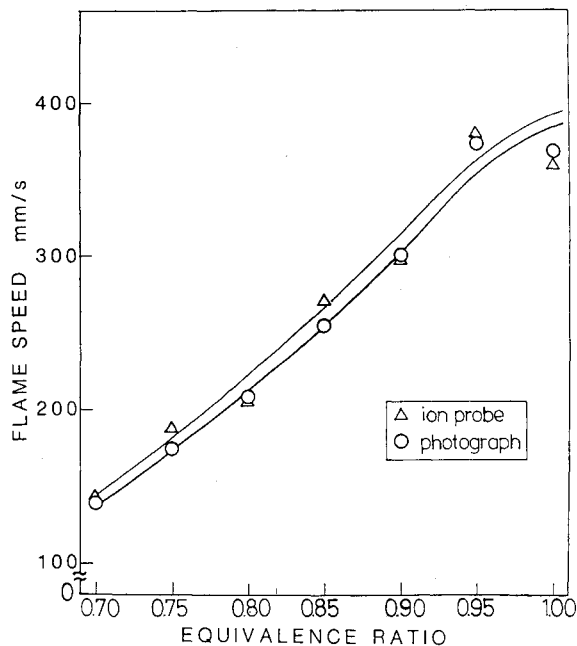
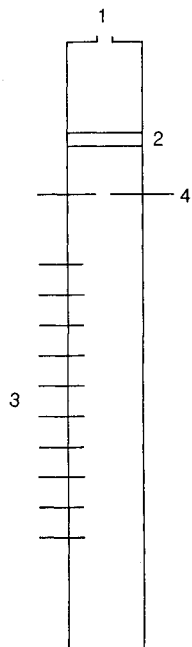


Fig. 3 Flame speeds of propane-air mixtures.

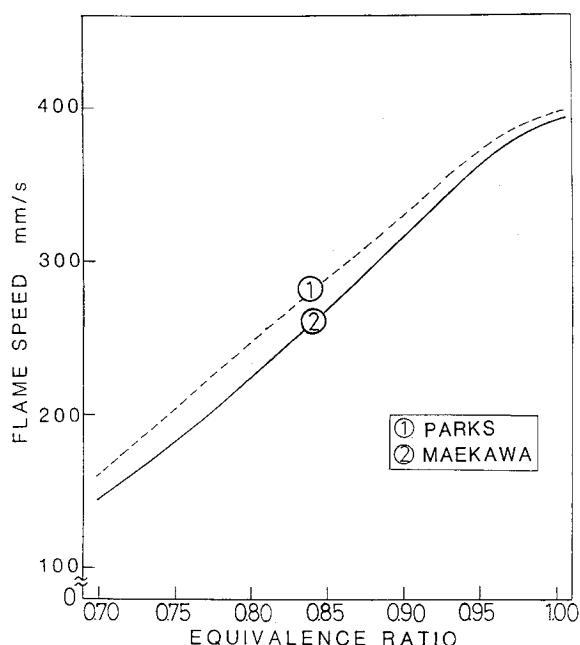


Fig. 4 Comparison of experimentally determined propane-air flame speeds from this and Parks investigations.

### Results and Discussion

When the combustible mixture in the tube with the nozzle and and screen in place was ignited by the electrodes, a flat flame was generated. After ignition the generated flame propagated about 100 mm down the tube, the flame flattened out and propagated another 400 mm, at which point the flat shape was lost. Figure 2 shows a multiexposure photograph of the flame propagation taken with a sector disk shutter. From the experiments, it was found that a combination of screen mesh, screen location, and nozzle diameter generated the flat flame as shown in Table 1. Figure 3 shows the results of propane-air flame speed measurements. The delta-marked curve shows the results of the ion probe measurements and the circle-marked curve those of photomeasurement. In Fig. 4, curve 1 is from the work of Parks and curve 2 was obtained in the present study. The speeds of curves 1 and 2 differ by 2-3%. Curve 1 of Fig. 4 shows a small difference compared with curve 2, reflecting the influence of the temperature. Curve 1 was obtained at about a temperature of 20°C. In this study, the experiments were done at an atmospheric temperature of 7°C. Generally, the flame speed increases with increasing temperature, so a temperature correction was made. With correction, curve 2 almost agrees with curve 1. When the flame gets farther from the screen, the velocity-flattening action in the tube is lost, the intervals of flat flame propagation become a smaller fraction of the total propagation time. And, the flat flames are no longer stable.

### Conclusions

This Note describes a new technique to measure the flame propagation rate in a cylindrical tube. It includes useful and interesting results that might be helpful to other researchers.

### References

- <sup>1</sup>Fristrom, R. M., "The Determination of Fundamental Burning Velocities of Hydrocarbons by a Revised Tube Method," *Physics of Fluids*, Vol. 8, 1965, p. 273.
- <sup>2</sup>Coward, H. F. and Hartwell, F. J., *Journal of the Chemical Society*, 1932, pp. 1996, 2676.
- <sup>3</sup>Gerstein, M., Levine, O., and Wong, E. L., *Journal of the American Chemical Society*, Vol. 73, 1951, p. 418.
- <sup>4</sup>Fuller, L. E., Parks, D. J., and Fletcher, E. A., "Flat Flames in Tubes—Easy Fundamental Flame Speed Measurements," *Combustion and Flame*, Vol. 13, 1969, p. 455.

## An Approximation of the Lowest Eigenfrequencies and Buckling Loads of Cylindrical and Conical Shell Panels Under Initial Stress

Detlef Teichmann\*

University of the Federal Armed Forces  
Munich, Federal Republic of Germany

### Introduction

THE vibrations of cylindrical and conical shells have been treated in a large number of publications<sup>1</sup> as have the vibrations of cylindrical shells and shell panels subjected to axial compression.<sup>2</sup> But only a few papers deal with the vibrations of conical shell panels under initial stress.<sup>3</sup>

The exact calculation of the eigenfrequencies of a shell requires, in most cases, a large amount of numerical computation. It is advantageous to the engineer to be able to study the influence of the most important parameters with a simple approximation, before he goes through expensive calculations. In this Note, an approximation formula for the calculation of vibrations of conical shells under initial stress will be derived.

### Shell Equations

The equations of motion for thin, shallow shells (Donnell-Mushtari-Koiter) under initial stress are

$$\nabla_{\alpha} N^{\alpha\beta} + p^{\beta} = \rho h \ddot{u}^{\beta}$$

$$b_{\alpha\beta} N^{\alpha\beta} + \nabla_{\alpha} (\dot{N}^{\alpha\beta} \nabla_{\beta} w) + \nabla_{\alpha} \nabla_{\beta} M^{\alpha\beta} = \rho h \ddot{w} \quad (1)$$

with the boundary conditions

$$u_{\beta} = 0, \text{ or } n_{\alpha} N^{\alpha\beta} = 0$$

$$w = 0, \text{ or } n_{\alpha} (\nabla_{\beta} M^{\alpha\beta} + \dot{N}^{\alpha\beta} \nabla_{\beta} w) = 0$$

$$\nabla_{\beta} w = 0, \text{ or } n_{\alpha} M^{\alpha\beta} = 0 \quad (2)$$

$M^{\alpha\beta}$ ,  $N^{\alpha\beta}$ ,  $\dot{N}^{\alpha\beta}$  denote the tensors of the moment, force, and initial force resultants;  $p^{\beta}$ ,  $p$  the surface loads;  $\ddot{u}^{\beta}$ ,  $\ddot{w}$  the tangential and normal accelerations;  $b_{\alpha\beta}$  the tensor of curvature;  $n_{\alpha}$  the components of direction vector;  $\rho$  the mass density;  $h$  the shell thickness, and  $\nabla_{\alpha}$  the covariant differentiation symbol.

### Cylindrical Shell Panel

For the vibrations of a cylindrical shell loaded only by normal stress in the direction of the generator (axial compression) and whose tangential inertia terms are neglected, one obtained from Eqs. (1) the well-known differential equations

$$r^2 u_{,ss} + \frac{1-\nu}{2} u_{,\theta\theta} + \frac{1+\nu}{2} r v_{,s\theta} + \nu r w_{,s} = 0$$

$$\frac{1+\nu}{2} r u_{,s\theta} + \frac{1-\nu}{2} r^2 v_{,ss} + v_{,\theta\theta} + w_{,\theta} = 0$$

$$-\nu r u_{,s} - v_{,\theta} - w - \frac{h^2 r^2}{12} \Delta \Delta w + \frac{\dot{N}_{ss}}{B} r^2 w_{,ss} = r^2 \frac{\rho h}{B} \ddot{w} \quad (3)$$

Received July 27, 1983. Copyright © American Institute of Aeronautics and Astronautics, Inc., 1985. All rights reserved.

\*Doctor of Engineering, Department of Aerospace Engineering.